Supporting Information

In-situ sampling of NOx emissions from US natural gas flares reveals heavy-tail emission characteristic

Genevieve Plant[1], Eric A. Kort[1], Alan M. Gorchov Negron[1,5], Yuanlei Chen[2], Graham Fordice[1,6], Colin Harkins[3,4]

[1] Climate and Space Sciences and Engineering, University of Michigan, Ann Arbor, MI 48109, United States

[2] Department of Energy Resources Engineering, Stanford University, Stanford, CA 94305, United States

[3] NOAA Chemical Sciences Laboratory (CSL), Boulder, CO, 80305, United States

[4] Cooperative Institute for Research in Environmental Sciences, University of Colorado, Boulder, CO 80309, United States

[5] Now at: Renewable and Sustainable Energy Institute, University of Colorado Boulder, Boulder, CO 80309, United States

[6] Now at: School for Environment and Sustainability, University of Michigan, Ann Arbor, MI 48109 United States

Supporting Information contains:

- 18 pages
- 6 tables
- 9 figures

1. Investigation of Potential Drivers

While not the focus of this works sampling design, we investigate possible correlations of NOx flare production with other parameters in our dataset. Using the prevailing wind direction over the targeted flight paths (see Fig.1), flare intercepts are approximately grouped as likely from the same flare. Note this grouping approach does not incorporate the potentially complex spatial transport of the plume, which we do not characterize with our wind measurements at the aircraft. We find no significant relationship between NOx emission factors and wind speed measured at the aircraft (Fig. S5). We do observe the trend that for flare plumes intercepted multiple times, the largest variability in NOx EF often coincides with higher average NOx EF (Fig. S6). Only in the Eagle Ford do we see a statistically significant relationship between NOx production and methane destruction removal efficiency (Fig. S7). The trend between higher observed variability and higher NOx, along with potential relationships between inefficient methane destruction and NOx emission factors suggest that some flares are malfunctioning and/or operating under conditions that result in performance deviations that are not captured in our current estimates of emissions from these sources.

Linkage of our airborne sampling of flare plumes to ground locations and flare metrics (gas volume, infrastructure age, etc.) is challenging due to potential complexity in the near-field transport of the flare plume, potential flare geolocation in other datasets (e.g. VIIRS), in addition to the connection of well-based information (e.g. Enverus[43]) and flare stack location. Despite the uncertainty in spatially linking these datasets, we explore possible relationships between flare NOx production and other factors such as flare volume and well age. While approximate we find no statistically significant correlation between NOx emission factor and flare volume and temperature in VIIRS (Fig. S8), or with well age and gas-to-oil ratio in Enverus (Fig. S9). This analysis does not eliminate these factors as potential drivers of flaring NOx emissions, but rather indicates that there is not a single, dominate explanatory variable in our observing framework. Further investigation into the root causes of heterogeneity in flare NOx production likely requires a different sampling and analysis strategy with more information about specific flare types and operation.

Figures

Tables

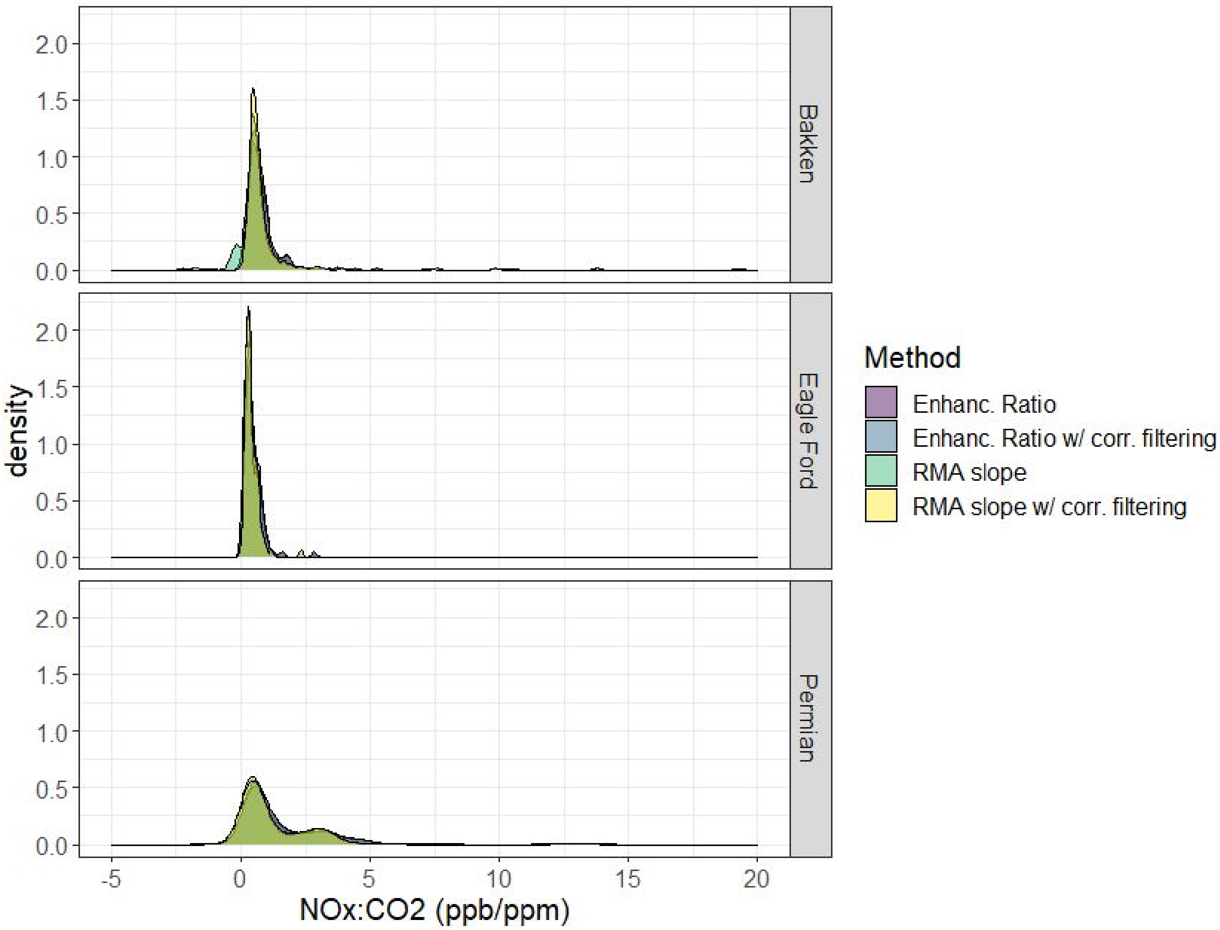

Figure S1. Observed NOx:CO_2 for the Bakken (top), Eagle Ford (middle), and Permian (bottom) using different analysis methods. Enhancement Ratios are calculated as the ratio of numerically integrated NOx and CO_2 enhancements, where the background value for each signal is determined by the 5th percentile of the data for each individual flare intercept. Model II ranged major axis (RMA) regressions are performed on the direct signals. A correlation filtering scheme is also applied to both approach, where the correlation between NO:CO_2 and NO_2:CO_2 is required to be greater than zero to warrant subsequent analysis. The various analysis methods agree well. The difference in mean value for between the enhancement ratio and slope (with positive correlation filtering) is 2%, 12%, and 7% for the Bakken, Eagle Ford, and Permian, respectively. The largest difference is with unfiltered RMA analysis, since it results in occasional negative slopes, pulling down the basin-wide average.

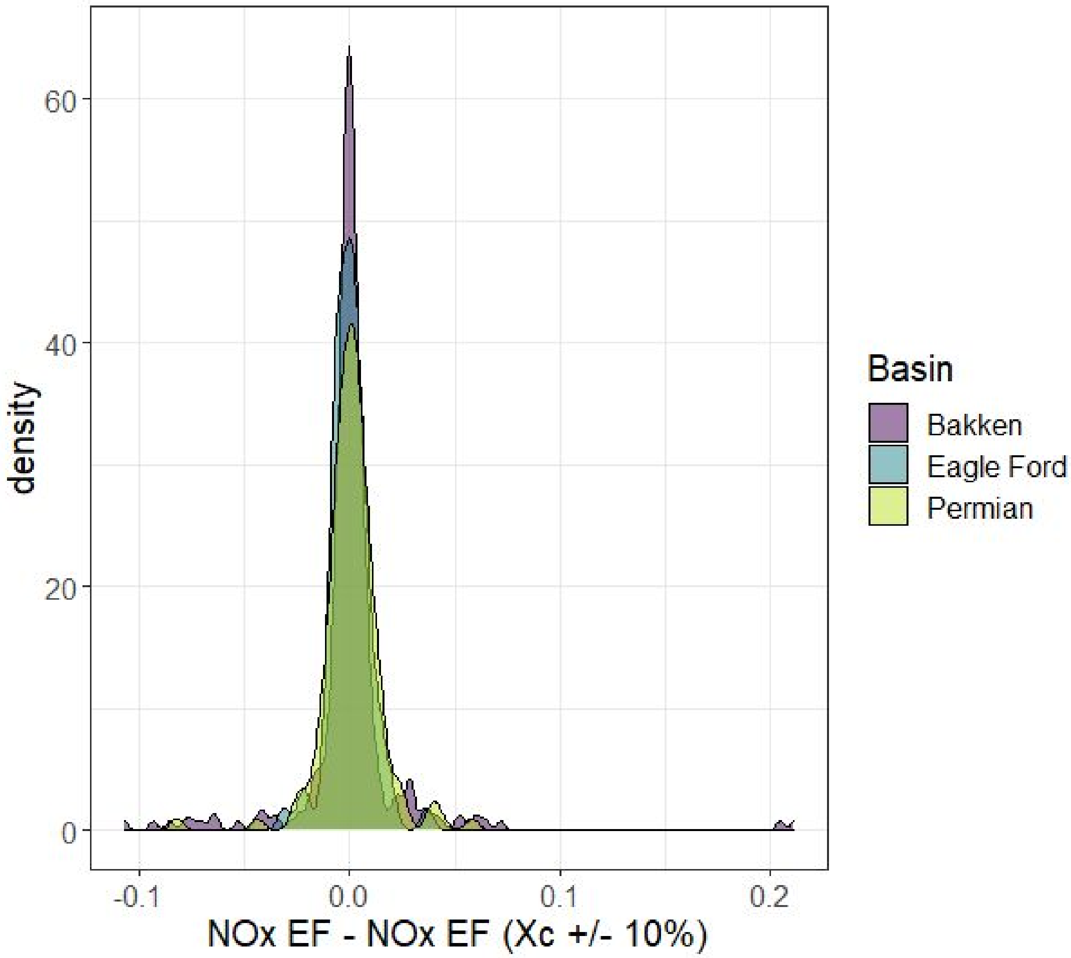

Figure S2. Normalized density of the difference in NOx EF when using Xc as defined in Table 1 of the main text and when the value is Xc is allowed to vary according to a Gaussian distribution with a standard deviation equal to +/- 10%. This standard deviation was chosen to mimic the range of gas compositions between basins. As the basin scale, the mean difference is 0.6, 0.2, and 0.6% and the median is 0.04, -0.5, and 0.6% for the Bakken, Eagle Ford, and Permian, respectively.

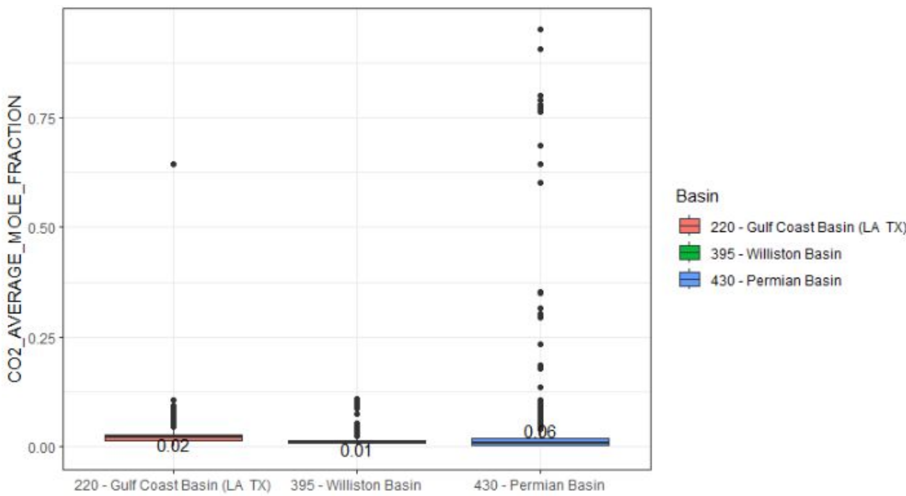

Figure S3. Greenhouse Gas Reporting Program (GHGRP) gas composition data (in terms of carbon dioxide, CO_2, content) for the Bakken (green, Williston Basin), Eagle Ford (red, Guld Coast Basin), and Permian (blue). Data Source: United States Environmental Protection Agency, GHG Reporting Program Data Sets: (2021), (available at https://www.epa.gov/ghgreporting/data-sets).

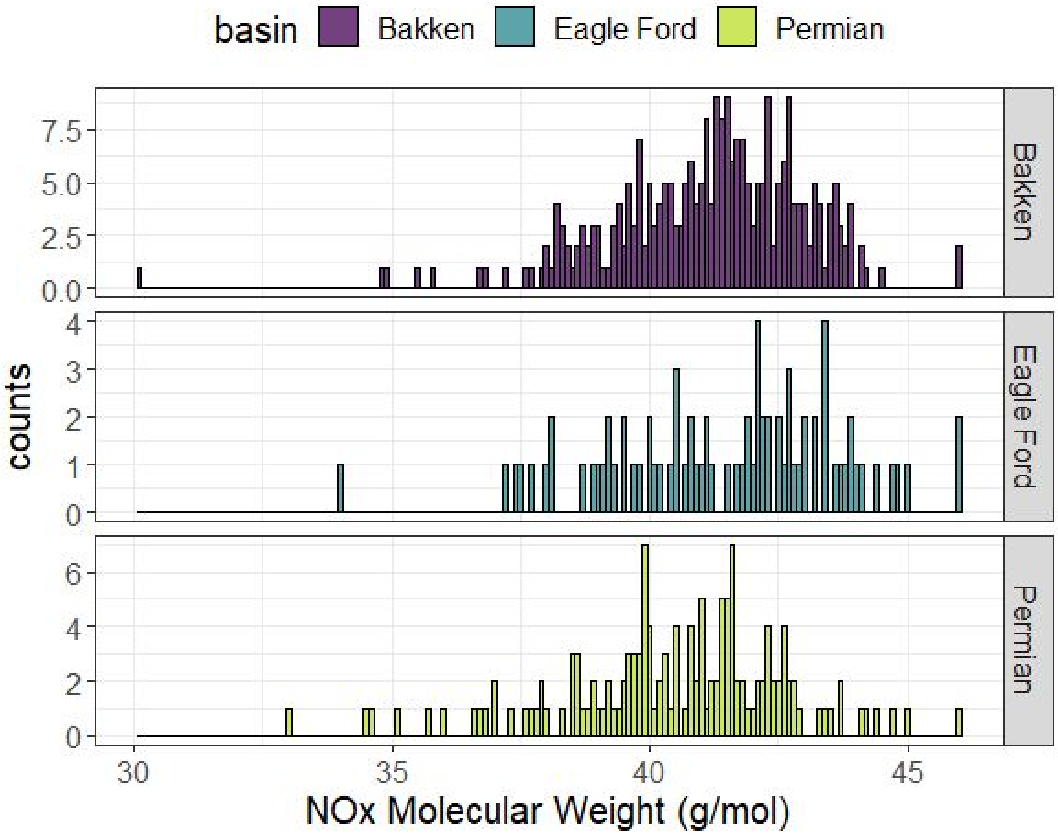

Figure S4. NOx molecular weights calculated using the observed NO:NO_2 slope, calculated using a model II ranged major axis regression. For the five intercepts where the NO:NO_2 slope was negative, a molecular weight of NO_2 was assigned.

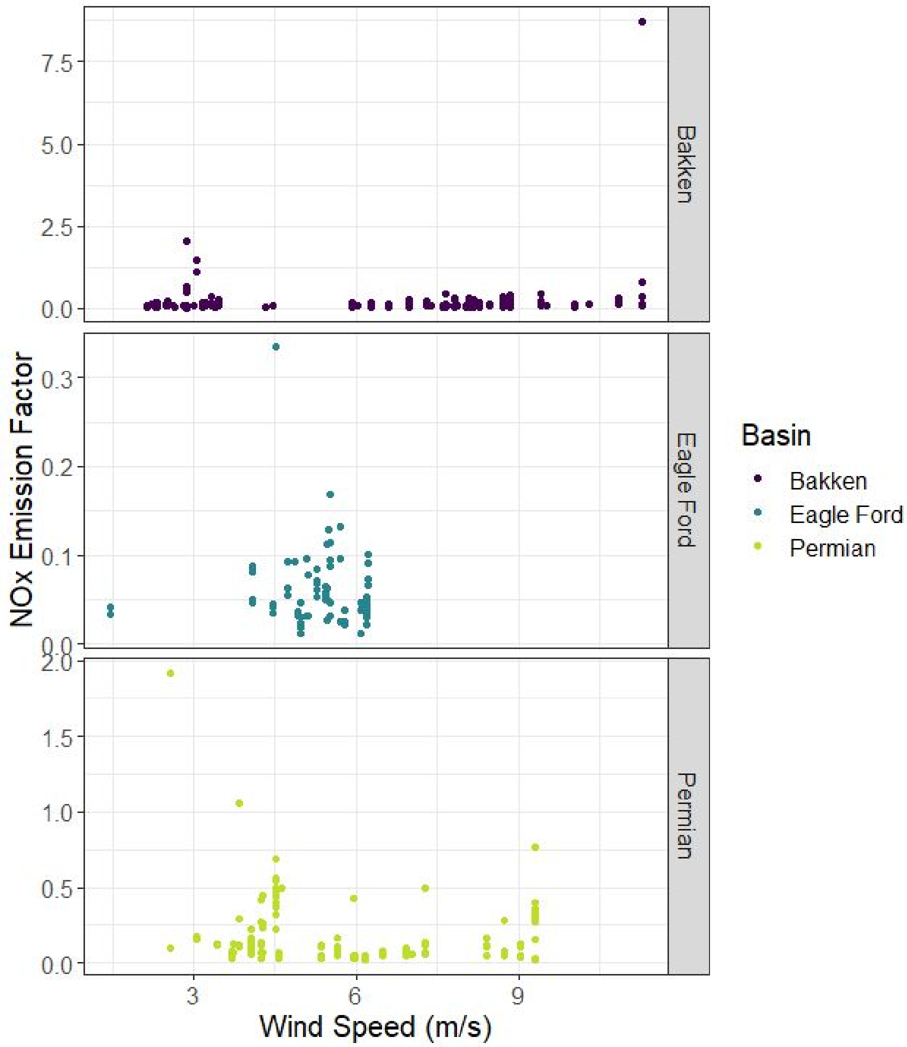

Figure S5. NOx emission factor (lb NOx/10^6 Btu) versus wind speed measured at the aircraft (m/s) for the Bakken (R^2<0.01, p=0.13), Eagle Ford (R^2<0.01, p=0.91), and Permian (R^2=0.05, p=0.008), where the R^2 and p-value (2-tailed parametric) correspond to an Ordinary Least Squares regression of the data for each basin. Ignoring the highest emission factor in the Bakken does not improve the statistical significance of the relationship between emission factor and wind speed measured at the aircraft (R^2<0.01, p=0.29).

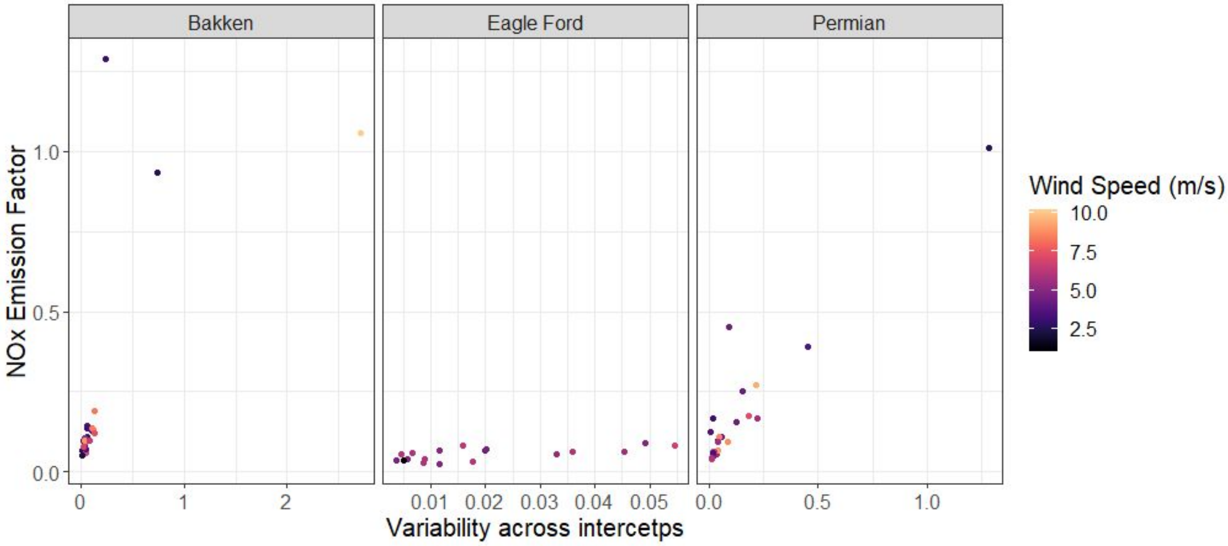

Figure S6. NOx emission factor (lb NOx/10^6 Btu) versus variability (i.e. standard deviation) across multiple intercepts within the same sampling region for the Bakken (R^2=0.46, p=1e-5), Eagle Ford (R^2=0.43, p=0.003), and Permian (R^2=0.87, p=8e-11), where the R^2 and p-value (2-tailed parametric) correspond to an Ordinary Least Squares regression of the data for each basin.

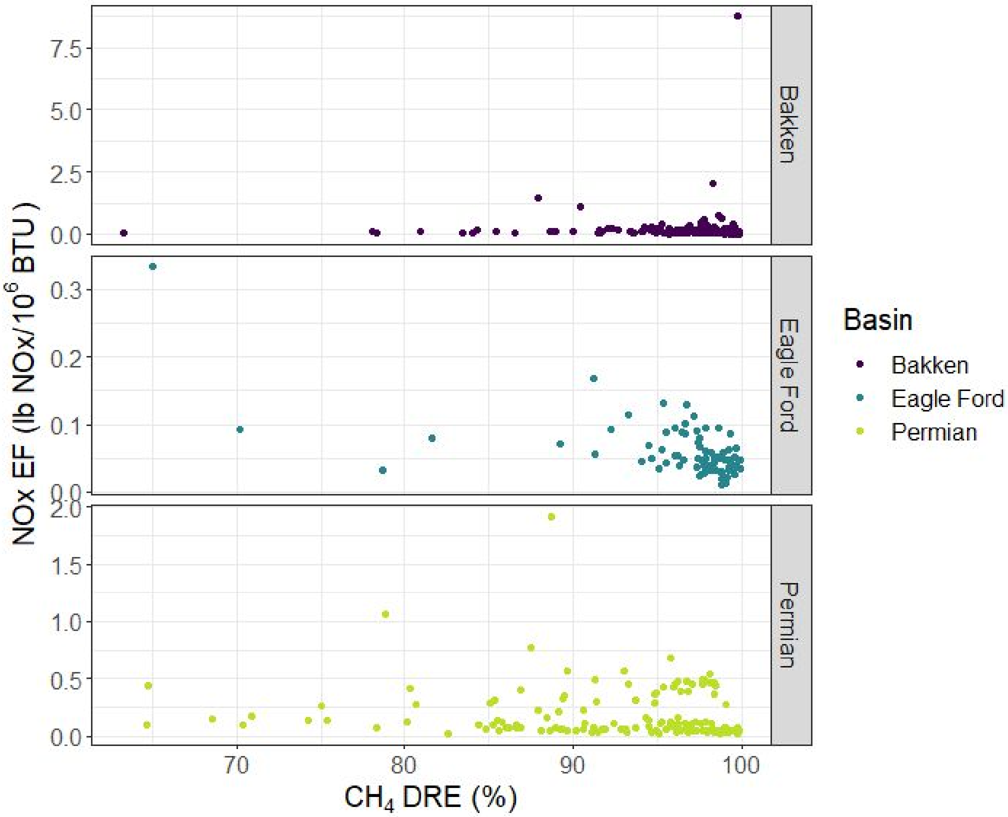

Figure S7. NOx emission factor (lb NOx/10^6 Btu) as a function of estimation methane destruction removal efficiency (as calculated in Plant et al. 2022) for the Bakken (R^2<0.01, p=0.96), Eagle Ford (R^2=0.38, p=2e-9), and Permian (R^2=0.01, p=0.24), where the R^2 and p-value (2-tailed parametric) correspond to an Ordinary Least Squares regression of the data for each basin.

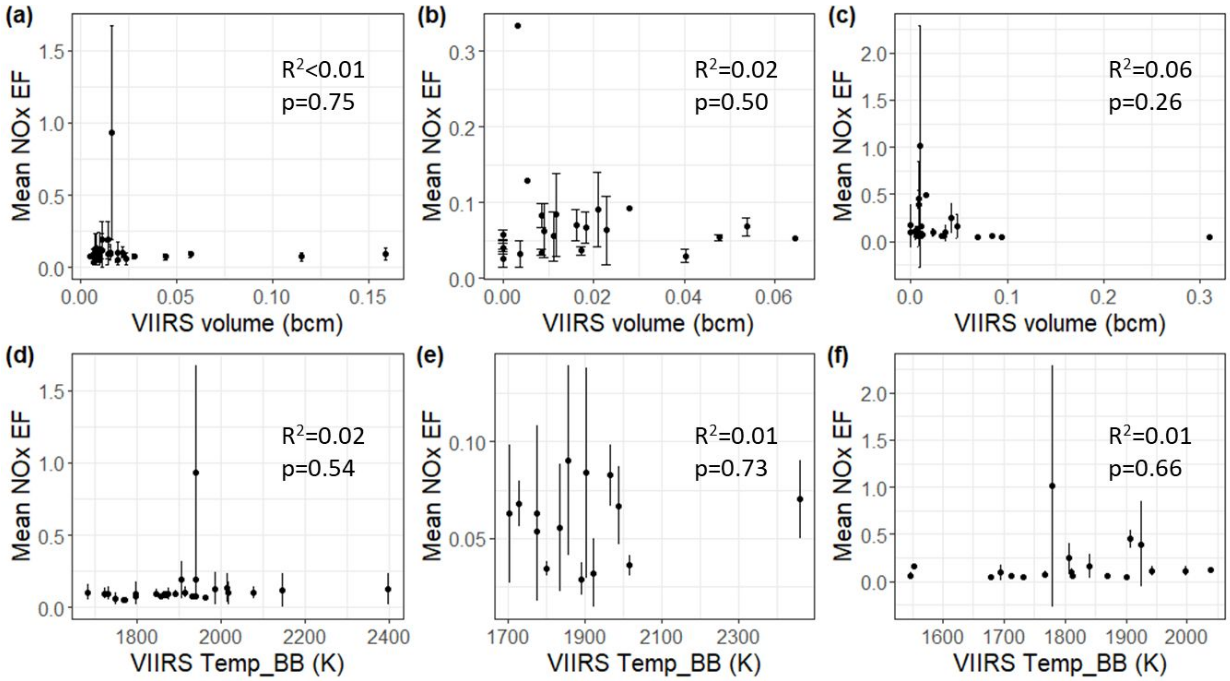

Figure S8. Observationally derived NOx emission factors (lb NOx/10^6 Btu) versus VIIRS-derived flare temperature and volume for the Bakken (panels a,d), Eagle Ford (panels b, e), and Permian (panels c,f).

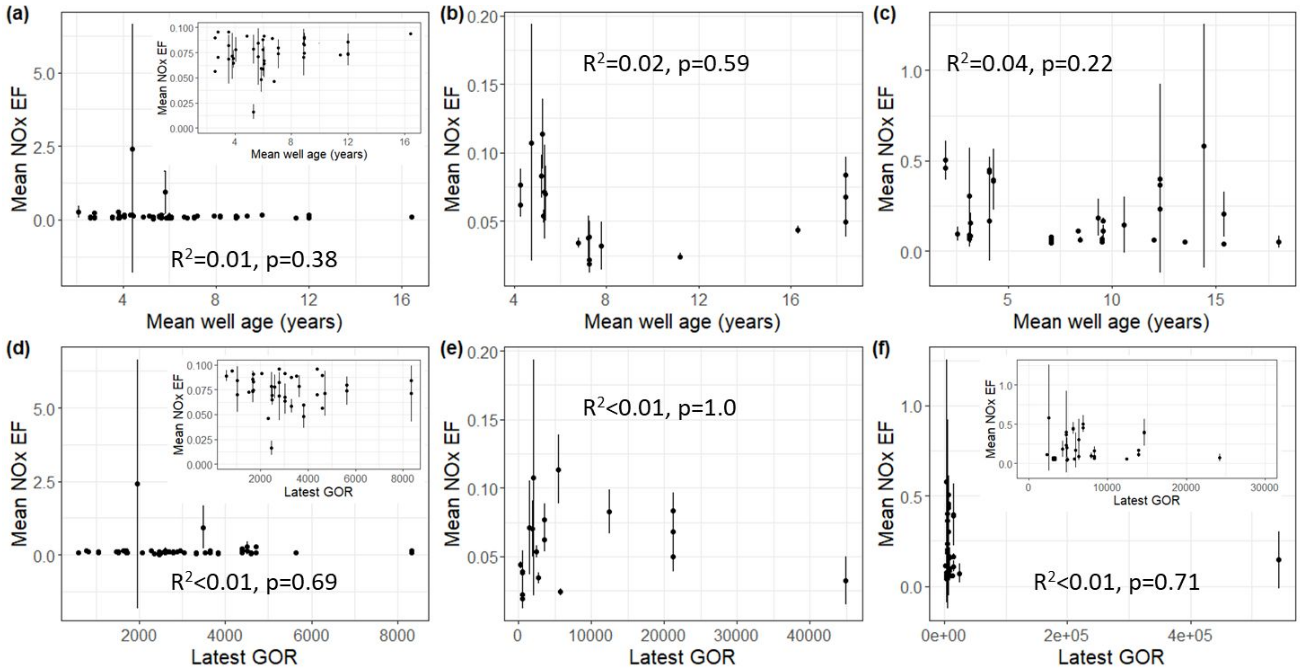

Figure S9. Observationally derived NOx emission factors (lb NOx/10^6 Btu) versus Enverus-linked well age and gas to oil ratio (GOR) for the Bakken (panels a,d), Eagle Ford (panels b, e), and Permian (panels c,f). Insets show zoomed in regions for panels with potential outliers.

Table S1. Basin Domain Definitions and Annual Flare Volumes

Basin	Domain Definition (°W, °N)	VIIRS 2020 annual Flare Volume (Bcm)
Bakken	105.5:102.3, 46.8:49.0	3.78
Eagle Ford	100.5:96.0, 27.7,29.9	1.60
Permian	104.8:100.3, 30.5:33.6	5.22

Table S2. F^3UEL airborne Sampling Statistics

Basin	# intercepts	# flares (pSize=0.002°)*	# NOx intercepts
Bakken	383	191	268
Eagle Ford	103	45	78
Permian	184	68	140
Total	**670**	**304**	**486**

* pSize (units = degrees) denotes the size (+/-) of the domain along the wind direction that is used to assign multiple plume intercepts to a single flare. The value of pSize was chosen based on examples where two flares were visually confirmed.

Table S3 – Summary Statistics of Observed NOx:CO_2 slopes (RMA slope, correlation>0)

	Mean	*Median*	*25^{th} Quantile*	*75^{th} Quantile*	*Minimum*	*Maximum*	*N*
Bakken	1.08	0.58	0.06	0.12	0.07	59.2	268
Eagle Ford	0.42	0.34	0.03	0.07	0.08	2.34	78
Permian	1.34	0.70	0.05	0.30	0.13	13.2	140

Table S4. NOx Emission Factors (EF) calculated using observationally-derived NOx molecular weight and assumption of NOx as NO_2.

	NOx Molecular Weight	Mean NOx EF	Median	Min	Max
Bakken **N = 268**	NO_2	0.159	0.086	0.0105	8.74
	Obs. NO:NO_2	0.133	0.077	0.010	5.72
Eagle Ford **N=78**	NO_2	0.060	0.049	0.011	0.334
	Obs. NO:NO_2	0.053	0.044	0.010	0.289
Permian **N=140**	NO_2	0.194	0.102	0.019	1.92
	Obs. NO:NO_2	0.169	0.092	0.016	1.66

Table S5. Basin-level NOx Flaring Emissions for 2020 compared to FOG Inventory.

Basin	***F^3UEL (metric ton/day) [95% CI]***	***FOG (metric ton/day)***
Bakken	33.8 [22.2, 54.6]	8.2
Eagle Ford	4.5 [3.6, 5.6]	3.6
Permian	52.2 [40.7, 65.1]	11.3

Table S6. Sectoral Breakdown of FOG NOx Inventory for 2020.

Basin	***Total NOx***	***Flaring***	***Drill Rigs***	***Dehydrators***	***Heaters***	***Artificial Lift***	***Lateral Compressors***	***Wellhead Compressors***
Bakken	34.7	8.2	13.8	0.3	1.0	8.5	2.7	0.2
Eagle Ford	86.4	3.6	18.3	0.8	2.5	10.1	7.1	44.0
Permian	276.1	11.3	71.6	2.3	7.5	56.6	19.8	107.0